Contents

List of Figures

List of Tables

Chapter 16

Maps, Strange Attractors, and Chaos

16.1 Motion on Resonant Tori

Consider an integrable Hamiltonian with two degrees of freedom. The energy $E(J_1, J_2)$ is then a function of the two action coordinates, so at fixed energy we may regard $J_2(J_1; E)$ as being determined by J_1. The motion is then given by $\phi_j(t) = \omega_j(J_1; E)\, t + \beta_j$, and, at fixed E, is confined to a two-torus $\mathbb{T}^2$ specified by the action J_1, as depicted in fig. 16.1. For a system with N freedoms (*i.e.* a phase space of dimension $2n$), integrable motion is confined to an n-torus $\mathbb{T}^N = \mathbb{S}^1 \times \cdots \times \mathbb{S}^1$. The frequencies $\omega_j = \partial E/\partial J_j = \omega_j(J_1, \ldots, J_{N-1}; E)$ are specified, at fixed E, by $N-1$ action variables. If, on a given torus, the frequency ratios $\omega_j/\omega_{j'}$ are rational numbers for all j and j', then the motion is periodic, and all frequencies are said to be in resonance. In this case we may write $\omega_j = k_j\, \omega_0$ for some set $\{k_1, \ldots, k_N\} \in \mathbb{Z}^N$, and some quantity ω_0 which has dimensions of frequency. One can Fourier decompose the original coordinates $q_\sigma(\phi, \boldsymbol{J})$ as

$$q_\sigma(\phi, \boldsymbol{J}) = \sum_{\boldsymbol{m}} \hat{q}_{\sigma, \boldsymbol{m}}(\boldsymbol{J})\, e^{i\boldsymbol{m}\cdot\phi} \quad , \tag{16.1}$$

and similarly for $p_\sigma(\phi, \boldsymbol{J})$, where $\boldsymbol{m} \in \mathbb{Z}^N$. Invoking the solution $\phi_\sigma(t) = k_\sigma \omega_0 t + \beta_\sigma$, one sees that the motion is periodic in time with period $T = 2\pi/\omega_0$. That all the frequencies are in resonance further means that for some of the $\boldsymbol{m}$ vectors, one has $\boldsymbol{m} \cdot \boldsymbol{k} = 0$.

16.1.1 The twist map

Consider the motion $\phi(t) = \boldsymbol{\omega}(\boldsymbol{J})\, t + \boldsymbol{\beta}$ along a resonant torus, and let us plot consecutive intersections of the trajectory with the (J_1, ϕ_1) plane, *i.e.* the subset of phase space where both E (or J_2) and ϕ_2 are fixed. Such a plot is called a *surface of section*. Successive intersections of this surface occur at time interval $\Delta t = 2\pi/\omega_2$, during which the angle ϕ_1 changes by $\Delta\phi_1 = \omega_1 \Delta t = 2\pi\alpha$, where $\alpha = \omega_1/\omega_2$. Focusing only on the surface of section, we write $\phi \equiv \phi_1$ and $J \equiv J_1$. The relation between (ϕ, J) values
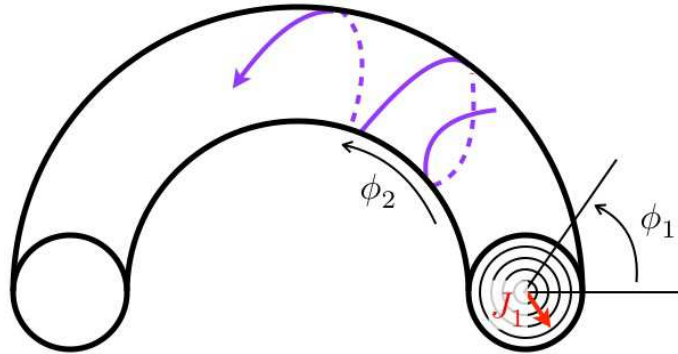
Figure 16.1: Motion of an $n = 2$ system on an invariant torus specified by action J_1, with $E(J_1, J_2)$ fixed.

at successive crossings of this surface is

$$\phi_{n+1} = \phi_n + 2\pi\alpha(J_{n+1})$$
$$J_{n+1} = J_n \quad .$$

(16.2)

Formally, we may write the map as $\boldsymbol{\varphi}_{n+1} = \hat{T}\boldsymbol{\varphi}_n$, where $\boldsymbol{\varphi}_n = (\phi_n, J_n)$ and $\hat{T}$ is the map. Note that the action variable is unchanged during the motion[1], and hence is fixed under the map. We are left with a mapping of the circle onto itself, called the *twist map*. Since the map faithfully represents Hamiltonian evolution, it must be canonical, meaning

$$\left\{\phi_{n+1}, J_{n+1}\right\}_{(\phi_n, J_n)} = \det \frac{\partial(\phi_{n+1}, J_{n+1})}{\partial(\phi_n, J_n)} = \frac{\partial\phi_{n+1}}{\partial\phi_n}\frac{\partial J_{n+1}}{\partial J_n} - \frac{\partial\phi_{n+1}}{\partial J_n}\frac{\partial J_{n+1}}{\partial\phi_n} = 1 \quad , \qquad (16.3)$$

which is indeed satisfied. If $\alpha(J) \in \mathbb{Q}$ is rational, certain iterations of the map leave the circle fixed. Specifically, let $\alpha = r/s$. Then $\hat{T}^s$ acts as the identity, leaving the entire circle (and indeed the entire (ϕ, J) plane) fixed.

For systems with N degrees of freedom, with (ϕ_N, J_N) or (ϕ_N, E) fixing the surface of section, one defines $\boldsymbol{\varphi} = (\phi_1, \ldots, \phi_{N-1})$ and $\boldsymbol{J} = (J_1, \ldots, J_{N-1})$, and with $\boldsymbol{\alpha} = (\omega_1/\omega_N, \ldots, \omega_{N-1}/\omega_N)$ one has

$$\boldsymbol{\varphi}_{n+1} = \boldsymbol{\phi}_n + 2\pi\boldsymbol{\alpha}(\boldsymbol{J}_{n+1})$$
$$\boldsymbol{J}_{n+1} = \boldsymbol{J}_n \quad .$$

(16.4)

One can check that this map is also area-preserving (canonical).

16.1.2   The perturbed twist map

Now consider a perturbed Hamiltonian $H(\boldsymbol{\phi}, \boldsymbol{J}) = H_0(\boldsymbol{J}) + \epsilon H_1(\boldsymbol{\phi}, \boldsymbol{J})$, again for $N = 2$. Once more we consider the surface of section defined by the (ϕ_1, J_1) plane. We expect a perturbed twist map $\hat{T}_\epsilon$ of the form

$$\phi_{n+1} = \phi_n + 2\pi\alpha(J_{n+1}) + \epsilon\, f(\phi_n, J_{n+1})$$
$$J_{n+1} = J_n + \epsilon\, g(\phi_n, J_{n+1}) \quad ,$$

(16.5)

---

[1]It is for this reason that we may write $\alpha(J_{n+1})$ in the first equation, rather than $\alpha(J_n)$. The reason will soon be apparent.

for some functions f and g. Is the perturbed twist map canonical? We could investigate this by computing the Poisson bracket $\{\phi_{n+1}, J_{n+1}\}$, but here we take another approach, which is to exhibit explicitly a type-II generator $F_2(\phi_n, J_{n+1})$ which effects the canonical transformation $(\phi_n, J_n) \to (\phi_{n+1}, J_{n+1})$. Consider the generator

$$F_2(\phi_n, J_{n+1}) = \phi_n J_{n+1} + 2\pi A(J_{n+1}) + \epsilon B(\phi_n, J_{n+1}) \quad . \tag{16.6}$$

The CT generated is

$$
\begin{aligned}
\phi_{n+1} &= \frac{\partial F_2}{\partial J_{n+1}} = \phi_n + 2\pi \frac{\partial A}{\partial J_{n+1}} + \epsilon \frac{\partial B}{\partial J_{n+1}} \\
J_n &= \frac{\partial F_2}{\partial \phi_n} = J_{n+1} + \epsilon \frac{\partial B}{\partial \phi_n} \quad .
\end{aligned}
\tag{16.7}
$$

We therefore identify $\alpha(J_{n+1}) = A'(J_{n+1})$ as well as

$$f(J_{n+1}, \phi_n) = \frac{\partial B}{\partial J_{n+1}} \quad , \qquad g(J_{n+1}, \phi_n) = -\frac{\partial B}{\partial \phi_n} \quad . \tag{16.8}$$

This, in turn, requires

$$\frac{\partial f}{\partial \phi_n} + \frac{\partial g}{\partial J_{n+1}} = 0 \quad , \tag{16.9}$$

which is a necessary and sufficient condition in order that the map $\hat{T}_\epsilon$ be canonical.

In the case $g = g(\phi_n)$, the above condition requires $f = f(J_{n+1})$, and we may absorb $f(J)$ into the definition of $\alpha(J)$. We then have the map

$$
\begin{aligned}
\phi_{n+1} &= \phi_n + 2\pi\alpha(J_{n+1}) \\
J_{n+1} &= J_n + \epsilon\, g(\phi_n) \quad .
\end{aligned}
\tag{16.10}
$$

For $\alpha(J) = J$ and $g(\phi) = -\sin\phi$, we obtain the *standard map*, about which we shall have more to say below.

16.2 From Time-Dependent Hamiltonian Systems to Maps

16.2.1 Parametric Oscillator

Consider the equation

$$\ddot{x} + \omega_0^2(t)\, x = 0 \quad , \tag{16.11}$$

where the oscillation frequency is a function of time. Equivalently,

$$\frac{d}{dt}\begin{pmatrix} x \\ \dot{x} \end{pmatrix} = \overbrace{\begin{pmatrix} 0 & 1 \\ -\omega_0^2(t) & 0 \end{pmatrix}}^{M(t)} \overbrace{\begin{pmatrix} x \\ \dot{x} \end{pmatrix}}^{\varphi(t)} \quad . \tag{16.12}$$

The formal solution is the path-ordered exponential,

$$\boldsymbol{\varphi}(t) = \mathcal{P} \exp \left\{ \int_0^t dt' \, M(t') \right\} \boldsymbol{\varphi}(0) \quad . \tag{16.13}$$

Let's consider an example in which

$$\omega(t) = \begin{cases} (1+\epsilon)\,\omega_0 & \text{if } 2n\tau \leq t < (2n+1)\tau \\[2mm] (1-\epsilon)\,\omega_0 & \text{if } (2n+1)\tau \leq t < (2n+2)\tau \quad . \end{cases} \tag{16.14}$$

Define $\boldsymbol{\varphi}_n \equiv \boldsymbol{\varphi}(2n\tau)$. Then

$$\boldsymbol{\varphi}_{n+1} = \exp(M_-\tau)\,\exp(M_+\tau)\,\boldsymbol{\varphi}_n \equiv \mathcal{U}\,\boldsymbol{\varphi}_n \quad , \tag{16.15}$$

where

$$M_\pm = \begin{pmatrix} 0 & 1 \\ -\omega_\pm^2 & 0 \end{pmatrix} \quad , \tag{16.16}$$

with $\omega_\pm \equiv (1\pm\epsilon)\,\omega_0$. Note that $M_\pm^2 = -\omega_\pm^2\,\mathbb{I}$ is a multiple of the identity. Evaluating the Taylor series for the exponential, one finds

$$\mathcal{U}_\pm \equiv \exp(M_\pm t) = \begin{pmatrix} \cos\omega_\pm\tau & \omega_\pm^{-1}\sin\omega_\pm\tau \\ -\omega_\pm\,\sin\omega_\pm\tau & \cos\omega_\pm\tau \end{pmatrix} \quad , \tag{16.17}$$

from which we derive the evolution matrix

$$\mathcal{U} \equiv \mathcal{U}_-\mathcal{U}_+ = \begin{pmatrix} \cos\omega_-\tau & \omega_-^{-1}\sin\omega_-\tau \\ -\omega_-\,\sin\omega_-\tau & \cos\omega_-\tau \end{pmatrix} \begin{pmatrix} \cos\omega_+\tau & \omega_+^{-1}\sin\omega_+\tau \\ -\omega_+\,\sin\omega_+\tau & \cos\omega_+\tau \end{pmatrix} \equiv \begin{pmatrix} a & b \\ c & d \end{pmatrix}$$

with

$$a = \cos\omega_-\tau\,\cos\omega_+\tau - \frac{\omega_+}{\omega_-}\sin\omega_-\tau\,\sin\omega_+\tau$$

$$b = \frac{1}{\omega_+}\cos\omega_-\tau\sin\omega_+\tau + \frac{1}{\omega_-}\sin\omega_-\tau\cos\omega_+\tau$$

$$\tag{16.18}$$

$$c = -\omega_+\,\cos\omega_-\tau\sin\omega_+\tau - \omega_-\,\sin\omega_-\tau\cos\omega_+\tau$$

$$d = \cos\omega_-\tau\,\cos\omega_+\tau - \frac{\omega_-}{\omega_+}\sin\omega_-\tau\,\sin\omega_+\tau \quad .$$

Note that $\mathcal{U}_\pm$ are each symplectic, hence $\det\exp(M_\pm\tau) = 1$, and therefore $\mathcal{U}$ is also symplectic with $\det\mathcal{U} = 1$. Also note that

$$P(\lambda) = \det\left(\mathcal{U} - \lambda\cdot\mathbb{I}\right) = \lambda^2 - T\lambda + \Delta \quad , \tag{16.19}$$

where $T = a + d = \operatorname{Tr}\mathcal{U}$ and $\Delta = ad - bc = \det\mathcal{U}$. The eigenvalues of $\mathcal{U}$ are

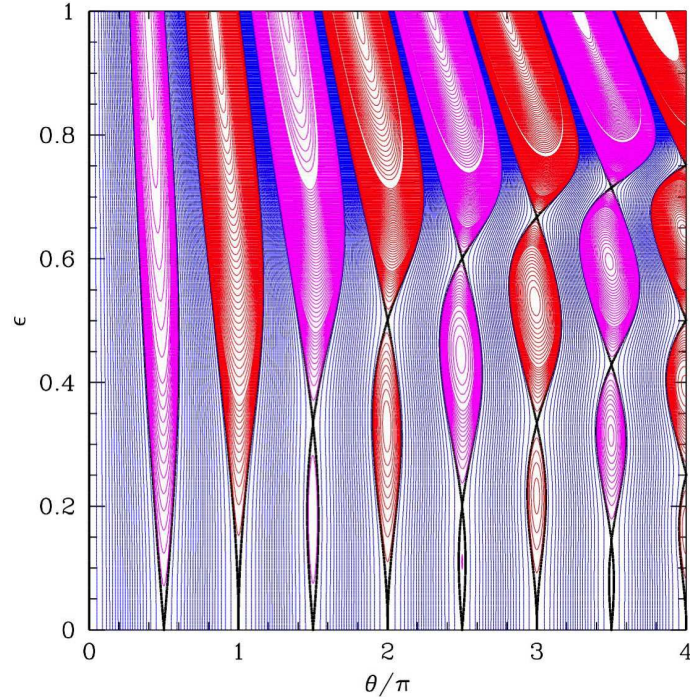$$\lambda_\pm = \tfrac{1}{2}T \pm \tfrac{1}{2}\sqrt{T^2 - 4\Delta} \quad . \tag{16.20}$$

Figure 16.2: Phase diagram for the parametric oscillator in the (θ, ϵ) plane. Thick black lines correspond to $T = \pm 2$. Blue regions: $|T| < 2$. Red regions: $T > 2$. Magenta regions: $T < -2$.

In our case, $\Delta = 1$. There are two cases to consider:

$$
\begin{aligned}
|T| < 2 &: \lambda_+ = \lambda_-^* = e^{i\delta} \quad , \quad \delta = \cos^{-1} \tfrac{1}{2} T \\
|T| > 2 &: \lambda_+ = \lambda_-^{-1} = \pm e^{\mu} \quad , \quad \mu = \cosh^{-1} \tfrac{1}{2} |T| \quad .
\end{aligned}
\tag{16.21}
$$

When $|T| < 2$, φ remains bounded; when $|T| > 2$, $|\varphi|$ increases exponentially with time. Note that phase space volumes are preserved by the dynamics.

To investigate more fully, let $\theta \equiv \omega_0 \tau$. The period of the frequency oscillations is $\Delta t = 2\tau$, i.e. $\omega_{\text{pump}} = \pi/\tau$ is the frequency at which the system is 'pumped', so

$$
\frac{\theta}{\pi} = \frac{\omega_0}{\omega_{\text{pump}}} = \frac{T_{\text{pump}}}{T_0} \quad ,
\tag{16.22}
$$

where $T_0 = 2\pi/\omega_0$ is the unperturbed natural frequency and $T_{\text{pump}} = \Delta t = 2\tau$. One finds $T = \text{Tr}\,\mathcal{U}$ is given by

$$
T = \frac{2\cos(2\theta) - 2\epsilon^2 \cos(2\epsilon\theta)}{1 - \epsilon^2} \quad .
\tag{16.23}
$$

We are interested in the boundaries in the (θ, ϵ) plane where $|T| = 2$. Setting $T = +2$, we write $\theta = n\pi + \delta$, which means $T_{\text{pump}} \approx n T_0$. Expanding for small δ and ϵ, we obtain the relation

$$
\delta^2 = n^2 \pi^2 \epsilon^4 \quad \Rightarrow \quad \epsilon = \pm \left| \frac{\delta}{n\pi} \right|^{1/2} \quad .
\tag{16.24}
$$

Setting $T = -2$, we write $\theta = (n + \frac{1}{2})\pi + \delta$, *i.e.* $T_{\text{pump}} \approx (n + \frac{1}{2}) T_0$. This gives

$$\delta^2 = \epsilon^2 \quad \Rightarrow \quad \epsilon = \pm\delta \quad . \tag{16.25}$$

The full phase diagram in the (θ, ϵ) plane is shown in fig. 16.2. A physical example is pumping a swing. By extending your legs periodically, you effectively change the length $\ell(t)$ of the pendulum, resulting in a time-dependent $\omega_0(t) = \sqrt{g/\ell(t)}$.

16.2.2   Kicked dynamics

A related model is described by the *kicked dynamics* of the Hamiltonian

$$H(t) = T(p) + V(q) K(t) \quad , \tag{16.26}$$

where

$$K(t) = \tau \sum_{n=-\infty}^{\infty} \delta(t - n\tau) \tag{16.27}$$

is the kicking function. The potential thus winks on and off with period τ. Note that

$$\lim_{\tau \to 0} K(t) = 1 \quad . \tag{16.28}$$

In the $\tau \to 0$ limit, the system is continuously kicked, and is equivalent to motion in a time-independent external potential $V(q)$.

The equations of motion are

$$\dot{q} = T'(p) \quad , \quad \dot{p} = -V'(q) K(t) \quad . \tag{16.29}$$

Integrating these equations, we obtain the map

$$\begin{aligned} q_{n+1} &= q_n + \tau\, T'(p_n) \\ p_{n+1} &= p_n - \tau\, V'(q_{n+1}) \quad , \end{aligned} \tag{16.30}$$

where $q_n = q(t = n\tau^+)$ and $p_n = p(t = n\tau^+)$. Note that the determinant of Jacobean of the map is unity:

$$\det \frac{\partial(q_{n+1}, p_{n+1})}{\partial(q_n, p_n)} = \det \begin{pmatrix} 1 & \tau\, T''(p_n) \\ -\tau\, V''(q_{n+1}) & 1 - \tau^2\, T''(p_n)\, V''(q_{n+1}) \end{pmatrix} = 1 \quad . \tag{16.31}$$

This means that the map preserves phase space volumes.

Consider, for example, the Hamiltonian $H(t) = \frac{L^2}{2I} - V\cos(\phi)\, K(t)$, where L is the angular momentum conjugate to ϕ. This results in the map

$$\begin{aligned} \phi_{n+1} &= \phi_n + 2\pi\epsilon\, J_n \\ J_{n+1} &= J_n - \epsilon \sin \phi_{n+1} \quad , \end{aligned} \tag{16.32}$$
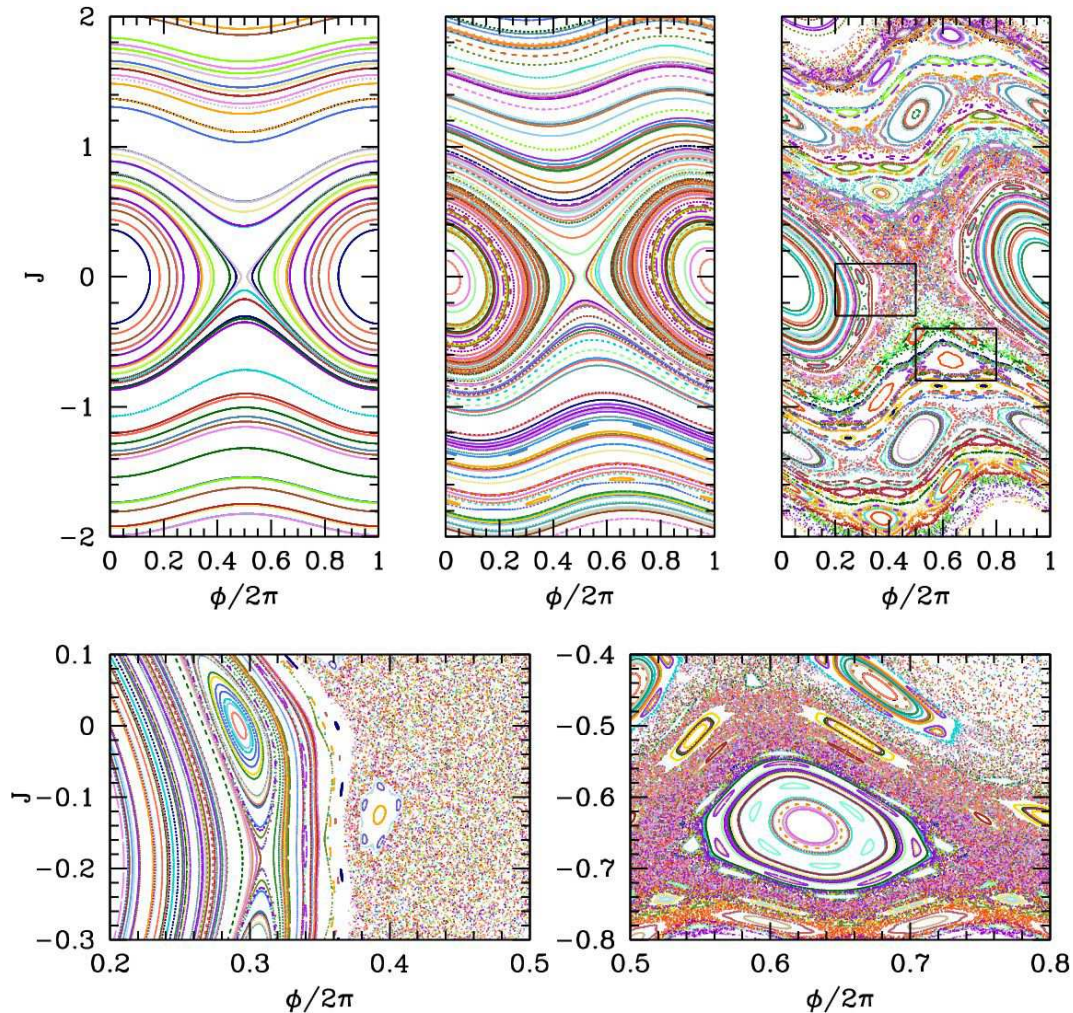
Figure 16.3: Top: the standard map, as defined in the text. Three values of the ϵ parameter are shown: $\epsilon = 0.01$ (left), $\epsilon = 0.2$ (center), and $\epsilon = 0.4$ (right). Bottom: details of the $\epsilon = 0.4$ map.

where $J_n = L_n / \sqrt{2\pi IV}$ and $\epsilon = \tau \sqrt{V/2\pi I}$. This is the standard map[2], which we encountered earlier, albeit in a slightly different form. In the limit $\epsilon \to 0$, we may define $\dot{\phi} = (\phi_{n+1} - \phi_n)/\epsilon$ and $\dot{J} = (J_{n+1} - J_n)/\epsilon$, and we recover the continuous time dynamics $\dot{\phi} = 2\pi J$ and $\dot{J} = -\sin\phi$. These dynamics preserve the energy function $E = \pi J^2 - \cos\phi$. There is a separatrix at $E = 1$, given by $J(\phi) = \pm\frac{2}{\pi}\left|\cos(\phi/2)\right|$. We see from fig. 16.3 that this separatrix is the first structure to be replaced by a chaotic fuzz as ϵ increases from zero to a small finite value.

Another well-studied system is the *kicked Harper model*, for which

$$H(t) = -V_1 \cos\left(\frac{2\pi p}{P}\right) - V_2 \cos\left(\frac{2\pi q}{Q}\right) K(t) \quad . \tag{16.33}$$

---

[2]The standard map us usually written in the form $x_{n+1} = x_n + \mathcal{J}_n$ and $\mathcal{J}_{n+1} = \mathcal{J}_n - k\sin(2\pi x_{n+1})$. We can recover our version by rescaling $\phi_n = 2\pi x_n$, $\mathcal{J}_n \equiv \sqrt{k}\, J_n$ and defining $\epsilon \equiv \sqrt{k}$.
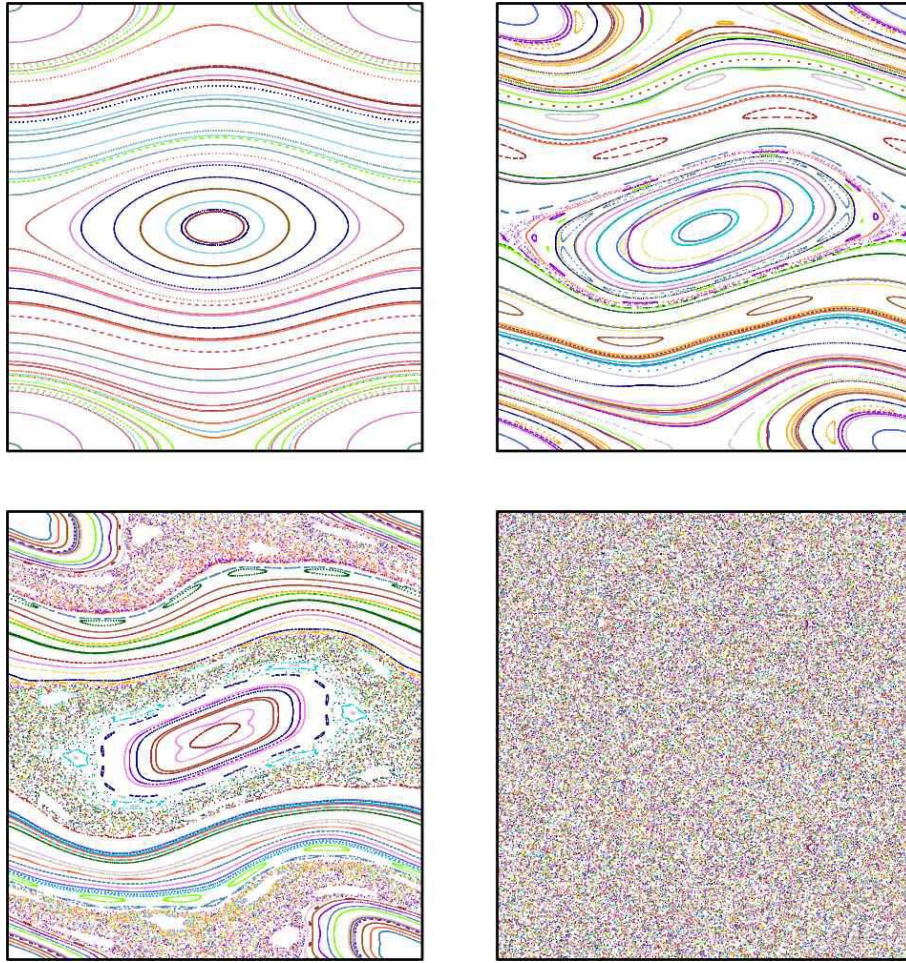
Figure 16.4: The kicked Harper map, with $\alpha = 2$, and with $\epsilon = 0.01$ (upper left), $\epsilon = 0.125$ (upper right), $\epsilon = 0.2$ (lower left) and $\epsilon = 5.0$ (lower right). The phase space here is the unit torus, $\mathbb{T}^2 = [0,1] \times [0,1]$.

With $x = q/Q$ and $y = p/P$, Hamilton's equations generate the map

$$
\begin{aligned}
x_{n+1} &= x_n + \epsilon\,\alpha\,\sin(2\pi y_n) \\
y_{n+1} &= y_n - \frac{\epsilon}{\alpha}\,\sin(2\pi x_{n+1}) \quad ,
\end{aligned}
\tag{16.34}
$$

where $\epsilon = 2\pi\tau\sqrt{V_1 V_2}/PQ$ and $\alpha = \sqrt{V_1/V_2}$ are dimensionless parameters. In this case, the conserved energy is

$$
E = -\alpha^{-1}\cos(2\pi x) - \alpha\cos(2\pi y) \quad .
\tag{16.35}
$$

There are then two separatrices, at $E = \pm(\alpha - \alpha^{-1})$, with equations $\alpha\cos(\pi y) = \pm\sin(\pi x)$ and $\alpha\sin(\pi y) = \pm\cos(\pi x)$. Again, as is apparent from fig. 16.4, the separatrix is the first structure to be destroyed at finite ϵ. This also occurs for the standard map – there is a transition to *global stochasticity* at a critical value of ϵ.

Note that the kicking function may be written as

$$K(t) = \tau \sum_{n=-\infty}^{\infty} \delta(t - n\tau) = \sum_{m=-\infty}^{\infty} \cos\left(\frac{2\pi m t}{\tau}\right) \quad , \tag{16.36}$$

a particularly handy result known as the *Poisson summation formula*. This, a kicked Hamiltonian may be written as

$$H(J, \phi, t) = H_0(J) + V(\phi) \sum_{m=-\infty}^{\infty} \cos\left(\frac{2\pi m t}{\tau}\right) \quad . \tag{16.37}$$

The $m = 0$ term generates the continuous time dynamics $\dot{\phi} = \omega_0(J)$, $\dot{J} = -V'(\phi)$. For the standard map, these are the dynamics of a simple pendulum. The $m \neq 0$ terms are responsible for resonances and the formation of so-called 'stochastic layers'.

16.3 Local Stability and Lyapunov Exponents

16.3.1 The fate of nearly separated initial conditions under iteration

Consider a map $\hat{T}$ acting on a phase space of dimension $2N$ (*i.e.* N position degrees of freedom). We ask what is the fate of two nearby initial conditions, $\boldsymbol{\xi}_0$ and $\boldsymbol{\xi}_0 + d\boldsymbol{\xi}$, under the iterated map. Under the first iteration, we have $\boldsymbol{\xi}_0 \to \boldsymbol{\xi}_1 = \hat{T}\boldsymbol{\xi}_0$ and

$$\boldsymbol{\xi}_0 + d\boldsymbol{\xi} \longrightarrow \boldsymbol{\xi}_1 + M(\boldsymbol{\xi}_0) \, d\boldsymbol{\xi} \quad , \tag{16.38}$$

where $M(\boldsymbol{\xi})$ is a matrix given by the *linearization of $\hat{T}$ at $\boldsymbol{\xi}$*, viz.

$$M_{ij}(\boldsymbol{\xi}) = \frac{\partial(\hat{T}\boldsymbol{\xi})_i}{\partial \xi_j} \quad . \tag{16.39}$$

Let's iterate again. Clearly $\boldsymbol{\xi}_1 \to \boldsymbol{\xi}_2 = \hat{T}^2 \boldsymbol{\xi}_0$ and

$$\boldsymbol{\xi}_1 + M(\boldsymbol{\xi}_0) \, d\boldsymbol{\xi} \longrightarrow \boldsymbol{\xi}_2 + M(\boldsymbol{\xi}_1) M(\boldsymbol{\xi}_0) \, d\boldsymbol{\xi} \quad . \tag{16.40}$$

After n iterations, we clearly have $\hat{T}^n \boldsymbol{\xi}_0 = \boldsymbol{\xi}_n$ and

$$\hat{T}^n(\boldsymbol{\xi}_0 + d\boldsymbol{\xi}) = \boldsymbol{\xi}_n + M(\boldsymbol{\xi}_{n-1}) \cdots M(\boldsymbol{\xi}_0) \, d\boldsymbol{\xi} \quad , \tag{16.41}$$

and we define $R^{(n)}(\boldsymbol{\xi}) = M\big(\hat{T}^n \boldsymbol{\xi}\big) \cdots M(\hat{T}\boldsymbol{\xi}) M(\boldsymbol{\xi})$, whose matrix elements may be written as $R_{ij}^{(n)}(\boldsymbol{\xi}) = \partial(\hat{T}^n \boldsymbol{\xi})_i / \partial \xi_j$.

Since the map $\hat{T}$ is presumed to be canonical, at each stage $M(\boldsymbol{\xi}_j) \in \mathsf{Sp}(2N)$, and since the product of symplectic matrices is a symplectic matrix, $R^{(n)}(\boldsymbol{\xi}) \in \mathsf{Sp}(2N)$. It is easy to see that for any real symplectic matrix R, the eigenvalues come in unimodular conjugate pairs $\{e^{i\delta}, e^{-i\delta}\}$, in real pairs $\{\lambda, \lambda^{-1}\}$ with $\lambda \in \mathbb{R}$, or in quartets $\{\lambda, \lambda^{-1}, \lambda^*, \lambda^{*-1}\}$ with $\lambda \in \mathbb{C}$, where λ^* is the complex conjugate of λ. This

follows from analysis of the characteristic polynomial $P(\lambda) = \det(\lambda - R)$ given the symplectic condition[3] $R^{\mathrm{t}}\,\mathbb{J}\,R = \mathbb{J}$. Let $\{\lambda_j^{(n)}(\boldsymbol{\xi})\}$ be the eigenvalues of $R^{(n)}(\boldsymbol{\xi})$, with $j \in \{1, \ldots, 2N\}$. One defines the *Lyapunov exponents*,

$$\nu_j(\boldsymbol{\xi}) = \lim_{n\to\infty} \frac{1}{n} \ln \left| \lambda_j^{(n)}(\boldsymbol{\xi}) \right| \quad . \tag{16.42}$$

These may be ordered such that $\nu_1 \leq \nu_2 \leq \cdots \leq \nu_{2N}$. Positive Lyapunov exponents correspond to an exponential stretching (as a function of the iteration number n), while negative ones correspond to an exponential squeezing.

As an example, consider the Arnol'd cat map, which is an automorphism of the torus $\mathbb{T}^2 = \mathbb{S}^1 \times \mathbb{S}^1$, given by[4]

$$\begin{aligned} q_{n+1} &= (K+1)\,q_n + p_n \\ p_{n+1} &= K q_n + p_n \quad , \end{aligned} \tag{16.43}$$

where $K \in \mathbb{Z}$, and where both q_n and p_n are defined modulo unity, so $(q_n, p_n) \in [0,1] \times [0,1]$. Note that K must be an integer in order for the map to be smooth on the torus, *i.e.* it is left unchanged by displacing either coordinate by an integer distance. The map is already linear, hence we can read off

$$M = \frac{\partial(q_{n+1}, p_{n+1})}{\partial(q_n, p_n)} = \begin{pmatrix} K+1 & 1 \\ K & 1 \end{pmatrix} \quad , \tag{16.44}$$

which is independent of (q_n, p_n). The inverse map also has integer coefficients:

$$M^{-1} = \begin{pmatrix} 1 & -1 \\ -K & K+1 \end{pmatrix} \quad . \tag{16.45}$$

Since $\det M = 1$, the cat map is canonical, *i.e.* it preserves phase space volumes. The eigenvalues of M are the roots of the characteristic polynomial $P(\lambda) = \lambda^2 - (K+2)\lambda - K$, and are given by

$$\lambda_\pm = 1 + \tfrac{1}{2}K \pm \sqrt{K + \tfrac{1}{4}K^2} \quad . \tag{16.46}$$

Thus, for $K \in \{-4, -3, -2, -1, 0\}$, the eigenvalues come in pairs $e^{\pm i\delta_K}$, with $\delta_{-4} = \pi$, $\delta_{-3} = \tfrac{2}{3}\pi$, $\delta_{-2} = \tfrac{1}{2}\pi$, $\delta_{-1} = \tfrac{1}{3}\pi$, and $\delta_0 = 0$. For $K < -4$ or $K > 0$, the eigenvalues are (λ, λ^{-1}) with $|\lambda| > 1$ and $0 < |\lambda|^{-1} < 1$, corresponding, respectively, to stretching and squeezing. The Lyapunov exponents are $\nu_\pm = \ln|\lambda_\pm|$.

16.3.2 Kolmogorov-Sinai entropy

Let $\Gamma < \infty$ be our phase space (at constant energy, for a Hamiltonian system), and $\{\Delta_j\}$ a partition of disjoint sets whose union is Γ. The simplest arrangement to think of is for each Δ_j to correspond to a little hypercube; stacking up all the hypercube builds the entire phase space. Now apply the inverse

---

[3] One has $P(\lambda) = \det(\lambda - R) = \det(\lambda - R^{\mathrm{t}}) = \det(\lambda + \mathbb{J}R^{-1}\mathbb{J}) = \det(\lambda^{-1} - R) \cdot \lambda^{2N}/\det R$ and therefore if λ is a root of the characteristic polynomial, then so is λ^{-1}. Since $R = R^*$, one also has $P(\lambda^*) = [P(\lambda)]^*$, hence if λ is a root, then so is λ^*. From $\mathrm{Pf}(R^{\mathrm{t}}\,\mathbb{J}\,R) = \det(R)\,\mathrm{Pf}(\mathbb{J})$, where Pf is the Pfaffian, one has $\det R = 1$.

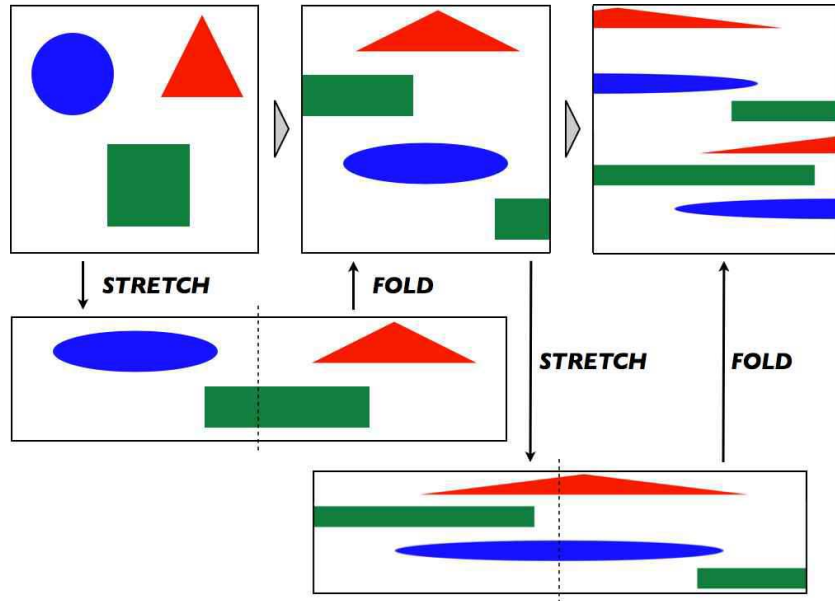[4] The map in eqn. 16.43 is a generalized version of Arnol'd's original cat map, which had $K = 1$.

Figure 16.5: The baker's transformation involves stretching/squeezing and 'folding' (cutting and restacking).

map $\hat{T}^{-1}$ to each Δ_j, and form the intersections $\Delta_{jk} \equiv \Delta_j \cap \hat{T}^{-1}\Delta_k$. If $\sum_j \mu(\Delta_j) = \mu(\Gamma) \equiv 1$, then $\sum_{j,k} \mu(\Delta_{jk}) = 1$. Iterating further, we obtain $\Delta_{jkl} \equiv \Delta_j \cap \hat{T}^{-1}\Delta_k \cap \hat{T}^{-2}\Delta_l$, *etc.*

The entropy of a distribution $\{p_a\}$ is defined to be $S = -\sum_a p_a \ln p_a$. Accordingly we define

$$S_L(\boldsymbol{\Delta}) = -\sum_{j_1} \cdots \sum_{j_L} \mu(\Delta_{j_1 \cdots j_L}) \ln \mu(\Delta_{j_1 \cdots j_L}) \quad . \tag{16.47}$$

This is a function of both the iteration number L as well as the initial set $\boldsymbol{\Delta} = \{\Delta_1, \ldots, \Delta_r\}$, where r is the number of subregions in our original partition. We then define the Kolmogorov-Sinai entropy to be

$$h_{\mathrm{KS}} \equiv \sup_{\boldsymbol{\Delta}} \lim_{L \to \infty} \frac{1}{L} S_L(\boldsymbol{\Delta}) \quad . \tag{16.48}$$

Here sup stands for *supremum*, meaning we maximize over all partitions $\boldsymbol{\Delta}$.

Consider, for example, the *baker's transformation* (see fig. 16.5), which stretches, cuts, stacks, and compresses the torus according to

$$(q', p') = \hat{T}(q, p) = \begin{cases} (2q, \frac{1}{2}p) & \text{if } 0 \le p < \frac{1}{2} \\ (2q - 1, \frac{1}{2}p + \frac{1}{2}) & \text{if } \frac{1}{2} \le p < 1 \end{cases} \tag{16.49}$$

It is not difficult to convince oneself that the KS entropy for the baker's transformation is $h_{\mathrm{KS}} = \ln 2$. On the other hand, for a simple translation map which takes $(q, p) \to (q', p') = (q + \alpha, p + \beta)$, it is easy to see that $h_{\mathrm{KS}} = 0$. The KS entropy is related to the Lyapunov exponents through the formula

$$h_{\mathrm{KS}} = \sum_j \nu_j \, \Theta(\nu_j) \quad . \tag{16.50}$$

The RHS is the sum over all the positive Lyapunov exponents $\gamma_j > 0$. Actually, this formula presumes that the γ_j do not vary in phase space, but in general this is not the case. The more general result is known as *Pesin's entropy formula*,

$$h_{\mathrm{KS}} = \int_\Gamma d\mu(\boldsymbol{\xi}) \sum_j \nu_j(\boldsymbol{\xi}) \, \Theta(\nu_j(\boldsymbol{\xi})) \quad . \tag{16.51}$$

16.4   The Poincaré-Birkhoff Theorem

Let's return to our discussion of the perturbed twist map,

$$\begin{pmatrix} \phi_{n+1} \\ J_{n+1} \end{pmatrix} = \hat{T}_\epsilon \begin{pmatrix} \phi_n \\ J_n \end{pmatrix} = \begin{pmatrix} \phi_n + 2\pi\alpha(J_{n+1}) + \epsilon f(\phi_n, J_{n+1}) \\ J_n + \epsilon g(\phi_n, J_{n+1}) \end{pmatrix} \quad , \tag{16.52}$$

with $\frac{\partial f}{\partial \phi_n} + \frac{\partial g}{\partial J_{n+1}} = 0$ in order that the map be canonical. For $\epsilon = 0$, the map $\hat{T}_0$ leaves J invariant, and takes circles to circles. If $\alpha(J) \neq \mathbb{Q}$, the images of the iterated map become dense on the circle.

Consider now a circle with fixed J for which $\alpha(J) = r/s$ is rational (may assume r and s are relatively prime), and without loss of generality let us presume $\alpha'(J) > 0$ so that on circles $J_\pm = J \pm \Delta J$ we have $\alpha(J_+) > r/s$ and $\alpha(J_-) < r/s$. Under $\hat{T}_0^s$, all the points on the circle $\mathcal{C} = \mathcal{C}(J)$ are fixed, whereas those on $\mathcal{C}_+$ rotate slightly counterclockwise, and those on $\mathcal{C}_-$ slightly clockwise (see left panel of fig. 16.6), where $\mathcal{C}_\pm = \mathcal{C}(J_\pm)$. Now consider the action of the iterated perturbed map $\hat{T}_\epsilon^s$. Acting on $\mathcal{C}_+$, the action is still a net counterclockwise shift (assuming $\epsilon \ll \frac{\Delta J}{J}$), with some small $\mathcal{O}(\epsilon)$ radial component. Similarly,
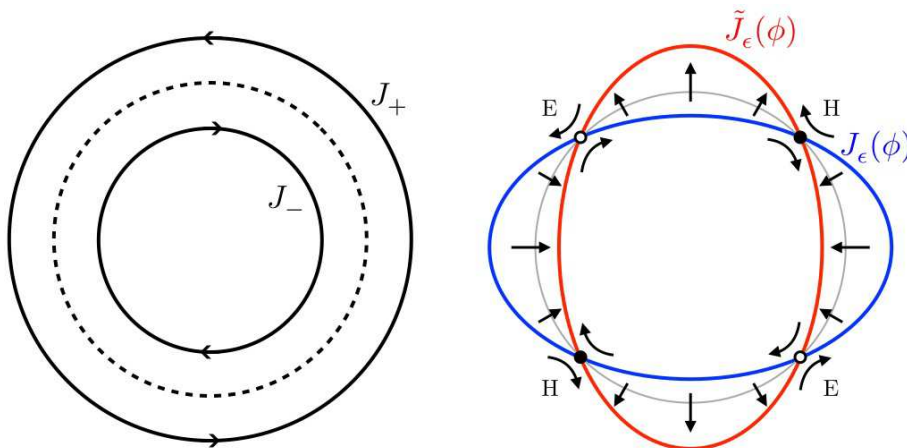

Figure 16.6: Left: The action of the iterated map $\hat{T}_0^s$ leaves the circle with $\alpha(J) = r/s$ invariant (dotted curve), but rotates slightly counterclockwise and clockwise on the circles $J = J_+$ and $J = J_-$, respectively. Right: The blue curve $J_\epsilon(\phi)$ is the locus of points where $\hat{T}_\epsilon^s$ acts purely radially and preserves ϕ, resulting in the red curve $\tilde{J}_\epsilon(\phi)$. Since $\hat{T}_\epsilon^s$ is volume-preserving, these curves must intersect in an alternating sequence of elliptic and hyperbolic fixed points.
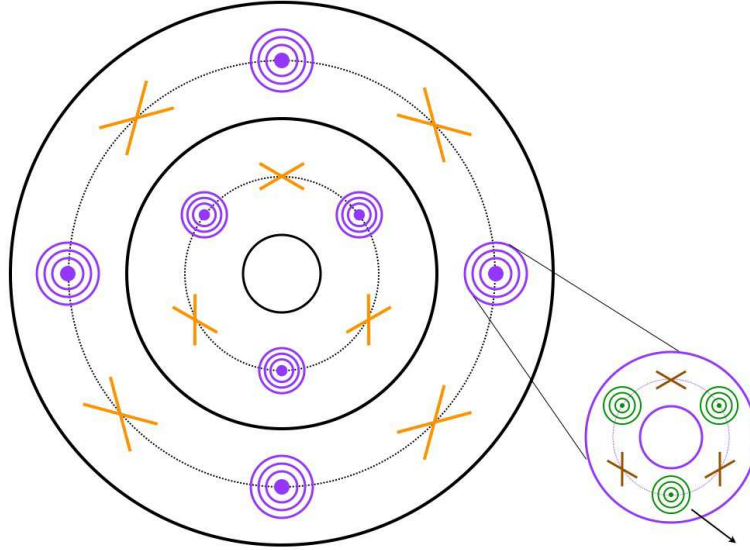
Figure 16.7: Self-similar structures in the iterated twist map.

acting on $\mathcal{C}_-$, the action is a net clockwise shift plus $\mathcal{O}(\epsilon)$ radial component. By the intermediate value theorem, for a given fixed ϕ, as one proceeds radially outward from $\mathcal{C}_-$ to $\mathcal{C}_+$, there must be a point $J = J_\epsilon(\phi)$ where the angular shift vanishes. This defines an entire curve $J_\epsilon(\phi)$ along which the action of $\hat{T}_\epsilon^s$ is purely radial. Now consider the curve $\tilde{J}_\epsilon(\phi) = \hat{T}_\epsilon^s J_\epsilon(\phi)$, *i.e.* the action of $\hat{T}_\epsilon^s$ on the curve $J_\epsilon(\phi)$. We know that each point along $J_\epsilon(\phi)$ is displaced radially, but we also know that $\hat{T}_\epsilon^s$ is volume-preserving. *Therefore, the curves $J_\epsilon(\phi)$ and $\tilde{J}_\epsilon(\phi)$ must intersect at an even number of points*[5]. These intersections are *fixed points* of the map $\hat{T}_\epsilon^s$. The situation is depicted in the right panel of fig. 16.6. From the figure, it is clear that the set $J_\epsilon(\phi) \cap \tilde{J}_\epsilon(\phi)$ consists of alternating elliptic and hyperbolic fixed points.

What we have just described is the content of the *Poincaré-Birkhoff theorem*: A small perturbation of a resonant torus with $\alpha(J) = r/s$ results in an equal number elliptic and hyperbolic fixed points for the iterated map $\hat{T}_\epsilon^s$. Since T_ϵ has period s acting on these fixed points, the number of EFPs and HFPs must be equal and also a multiple of s. In the vicinity of the EFPs, this structure repeats, as depicted above in fig. 16.7.

Stable/unstable manifolds and homoclinic/heteroclinic intersections

Now consider the HFPs. Emanating from a given HFP $\boldsymbol{\xi}^*$ are *stable and unstable manifolds*, $\Sigma^{\mathrm{S/U}}(\boldsymbol{\xi}^*)$, defined by:

$$
\begin{aligned}
\boldsymbol{\xi} \in \Sigma^{\mathrm{S}}(\boldsymbol{\xi}^*) &\Rightarrow \lim_{n\to\infty} \hat{T}_\epsilon^{+ns}\boldsymbol{\xi} = \boldsymbol{\xi}^* \quad \text{(to } \boldsymbol{\xi}^*\text{)} \\
\boldsymbol{\xi} \in \Sigma^{\mathrm{U}}(\boldsymbol{\xi}^*) &\Rightarrow \lim_{n\to\infty} \hat{T}_\epsilon^{-ns}\boldsymbol{\xi} = \boldsymbol{\xi}^* \quad \text{(from } \boldsymbol{\xi}^*\text{)} \quad .
\end{aligned}
\tag{16.53}
$$

Note that $\Sigma^{\mathrm{U}}(\boldsymbol{\xi}_i^*)$ can never intersect $\Sigma^{\mathrm{U}}(\boldsymbol{\xi}_j^*)$ for any i and j, nor can $\Sigma^{\mathrm{S}}(\boldsymbol{\xi}_i^*)$ ever intersect $\Sigma^{\mathrm{S}}(\boldsymbol{\xi}_j^*)$. However, $\Sigma^{\mathrm{U}}(\boldsymbol{\xi}_i^*)$ *can* intersect $\Sigma^{\mathrm{S}}(\boldsymbol{\xi}_j^*)$. If $i = j$, such an intersection is called a *homoclinic point*, while for

---

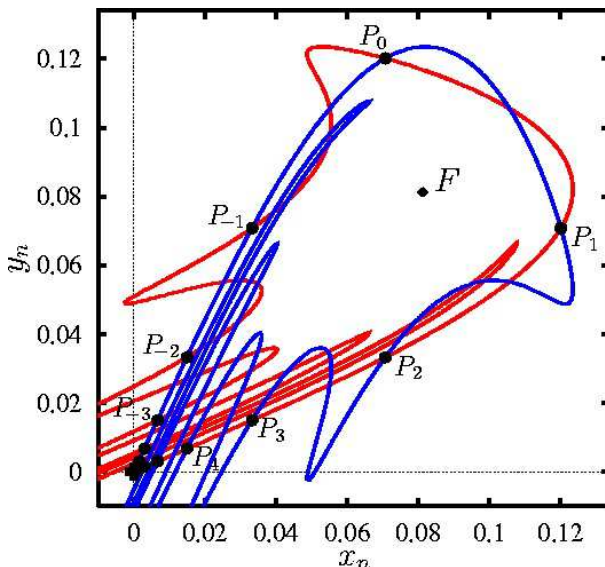[5]Tangency is nongeneric and broken by a small change in ϵ.

Figure 16.8: Homoclinic tangle for the map $x_{n+1} = y_n$ and $y_{n+1} = (a + by_n^2)\,y_n - x_n$ for parameters $a = 2.693$, $b = -104.888$. Stable (blue) and unstable (red) manifolds emanating from the HFP at $(0,0)$ are shown.

$i \neq j$ the intersection is called a *heteroclinic point*. Because $\hat{T}_\epsilon^s$ is continuous and invertible, its action at a homoclinic/heteroclinic point will produce a *new* homoclinic/heteroclinic point, *ad infinitum*! For homoclinic intersections, the resulting structure is known as a *homoclinic tangle*, an example of which is shown in fig. 16.8.

16.5   One-dimensional Maps

Consider now an even simpler case of a purely one-dimensional map,

$$x_{n+1} = f(x_n) \quad . \tag{16.54}$$

A fixed point of the map satisfies $x = f(x)$. Writing the solution as x^* and expanding about the fixed point, we write $x = x^* + u$ and obtain

$$u_{n+1} = f'(x^*)\,u_n + \mathcal{O}(u^2) \quad . \tag{16.55}$$

Thus, the fixed point is stable if $\left| f'(x^*) \right| < 1$, since successive iterates of u then get smaller and smaller. The fixed point is unstable if $\left| f'(x^*) \right| > 1$.

Perhaps the most important and most studied of the one-dimensional maps is the logistic map, where $f(x) = rx(1 - x)$, defined on the interval $x \in [0, 1]$. This has a fixed point at $x^* = 1 - r^{-1}$ if $r > 1$. We then have $f'(x^*) = 2 - r$, so the fixed point is stable if $r \in (1, 3)$. What happens for $r > 3$? We can explore the behavior of the iterated map by drawing a *cobweb diagram*, shown in fig. 16.9. We sketch, on the same graph, the curves $y = x$ (in blue) and $y = f(x)$ (in black). Starting with a point x on the line
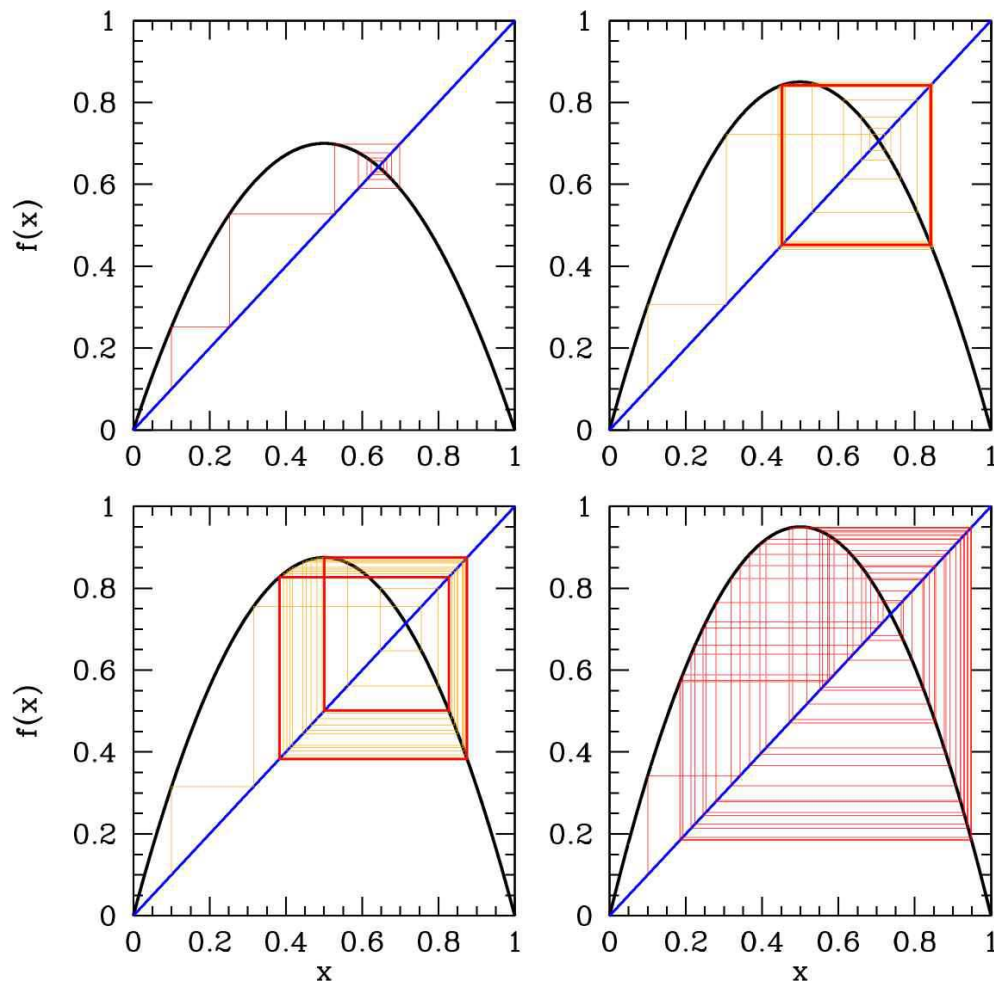
Figure 16.9: Cobweb diagram showing iterations of the logistic map $f(x) = rx(1-x)$ for $r = 2.8$ (upper left), $r = 3.4$ (upper right), $r = 3.5$ (lower left), and $r = 3.8$ (lower right). Note the single stable fixed point for $r = 2.8$, the stable two-cycle for $r = 3.4$, the stable four-cycle for $r = 3.5$, and the chaotic behavior for $r = 3.8$.

$y = x$, we move vertically until we reach the curve $y = f(x)$. To iterate, we then move horizontally to the line $y = x$ and repeat the process. We see that for $r = 3.4$ the fixed point x^* is unstable, but there is a stable two-cycle, defined by the equations

$$x_2 = rx_1(1 - x_1)$$
$$x_1 = rx_2(1 - x_2) \quad . \tag{16.56}$$

The second iterate of $f(x)$ is then

$$f^{(2)}(x) = f\big(f(x)\big) = r^2 x(1-x)\big(1 - rx + rx^2\big) \quad . \tag{16.57}$$

Setting $x = f^{(2)}(x)$, we obtain a cubic equation. Since $x - x^*$ must be a factor, we can divide out by this
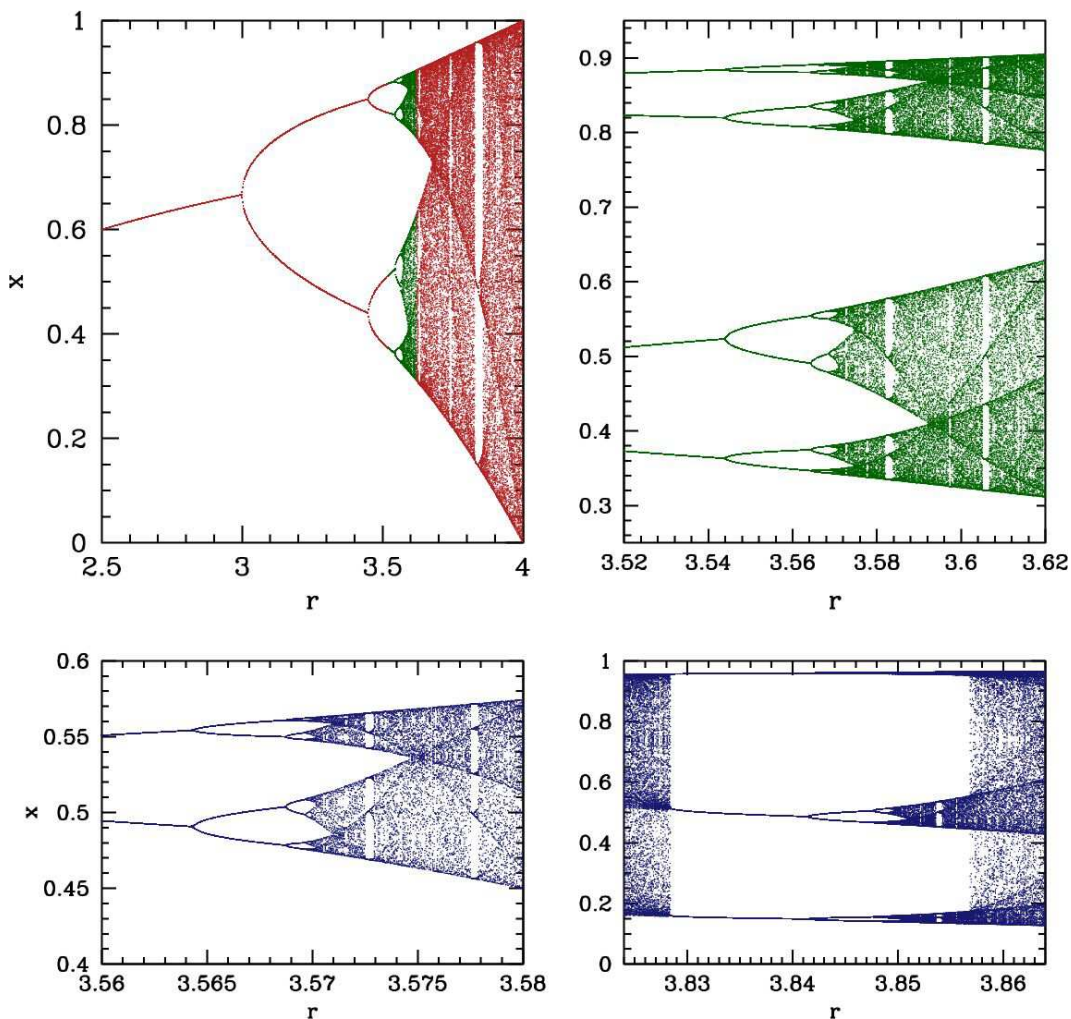
Figure 16.10: Iterates of the logistic map $f(x) = rx(1-x)$.

monomial and obtain a quadratic equation for x_1 and x_2. We find

$$x_{1,2} = \frac{1 + r \pm \sqrt{(r+1)(r-3)}}{2r} \quad . \tag{16.58}$$

How stable is this 2-cycle? We find

$$\frac{d}{dx} f^{(2)}(x) = r^2(1 - 2x_1)(1 - 2x_2) = -r^2 + 2r + 4 \quad . \tag{16.59}$$

The condition that the 2-cycle be stable is then

$$-1 < r^2 - 2r - 4 < 1 \quad \Longrightarrow \quad r \in \left[3, 1 + \sqrt{6}\right] \quad . \tag{16.60}$$

At $r = 1 + \sqrt{6} = 3.4494897\ldots$ there is a bifurcation to a 4-cycle, as can be seen in fig. 16.10.
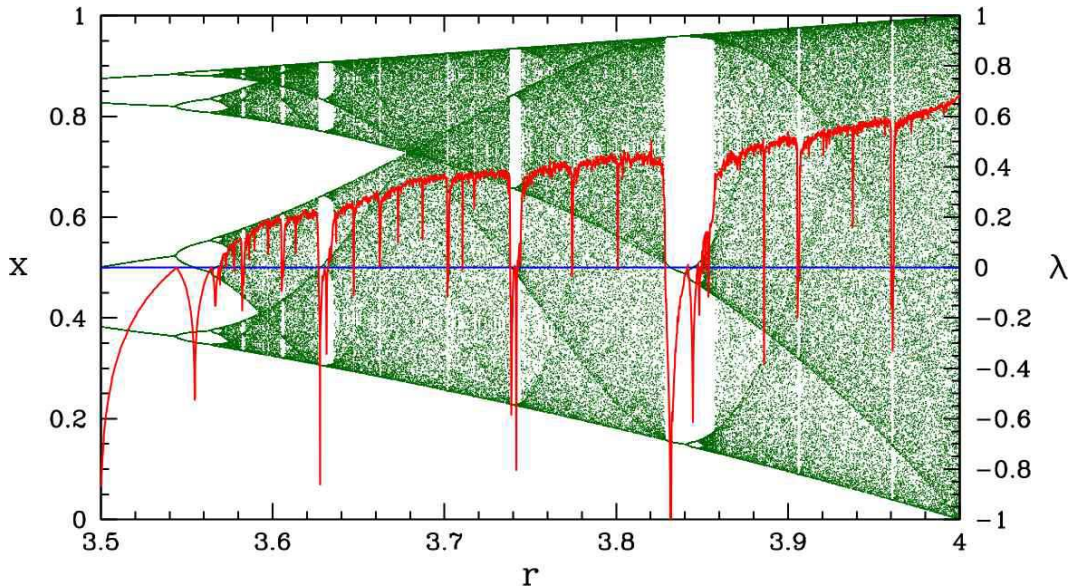
Figure 16.11: Lyapunov exponent (in red) for the logistic map.

16.5.1 Lyapunov Exponents

The *Lyapunov exponent* $\lambda(x)$ of the iterated map $f(x)$ at point x is defined to be

$$\lambda(x) = \lim_{n\to\infty} \frac{1}{n} \ln \left| \frac{df^{(n)}(x)}{dx} \right| = \lim_{n\to\infty} \frac{1}{n} \sum_{j=1}^{n} \ln \left| f'(x_j) \right| \quad , \tag{16.61}$$

where $x_{j+1} \equiv f(x_j)$. The significance of the Lyapunov exponent is the following. If $\mathrm{Re}\big(\lambda(x)\big) > 0$ then two initial conditions near x will exponentially separate under the iterated map. For the *tent map*,

$$f(x) = \begin{cases} 2rx & \text{if } x < \frac{1}{2} \\ 2r(1-x) & \text{if } x \ge \frac{1}{2} \end{cases} , \tag{16.62}$$

one easily finds $\lambda(x) = \ln(2r)$ independent of x. Thus, if $r > \frac{1}{2}$ the Lyapunov exponent is positive, meaning that every neighboring pair of initial conditions will eventually separate exponentially under repeated application of the map. The Lyapunov exponent for the logistic map is depicted in fig. 16.11.

16.5.2 Chaos in the logistic map

What happens in the logistic map for $r > 1 + \sqrt{6}$? At this point, the 2-cycle becomes unstable and a stable 4-cycle develops. However, this soon goes unstable and is replaced by a stable 8-cycle, as the right hand panel of fig. 16.10 shows. The first eight values of r where bifurcations occur are given by

$$\begin{aligned} r_1 &= 3 \quad , \; r_2 = 1 + \sqrt{6} = 3.4494897 \quad , \; r_3 = 3.544096 \quad , \; r_4 = 3.564407 \quad , \\ r_5 &= 3.568759 \quad , \; r_6 = 3.569692 \quad , \; r_7 = 3.569891 \quad , \; r_8 = 3.569934 \quad , \dots \end{aligned} \tag{16.63}$$

Feigenbaum noticed that these numbers seemed to be converging exponentially. With the *Ansatz*

$$r_\infty - r_k = \frac{c}{\delta^k} \quad , \tag{16.64}$$

one finds

$$\delta = \frac{r_k - r_{k-1}}{r_{k+1} - r_k} \quad , \tag{16.65}$$

and taking the limit $k \to \infty$ from the above data one finds

$$\delta = 4.669202 \quad , \quad c = 2.637 \quad , \quad r_\infty = 3.5699456 \quad . \tag{16.66}$$

There's a very nifty way of thinking about the chaos in the logistic map at the special value $r = 4$. If we define $x_n \equiv \sin^2 \theta_n$, then we find

$$\theta_{n+1} = 2\theta_n \quad . \tag{16.67}$$

Now let us write

$$\theta_0 = \pi \sum_{k=1}^{\infty} \frac{b_k}{2^k} \quad , \tag{16.68}$$

where each b_k is either 0 or 1. In other words, the $\{b_k\}$ are the digits in the binary decimal expansion of θ_0 / π. Now $\theta_n = 2^n \theta_0$, hence

$$\theta_n = \pi \sum_{k=1}^{\infty} \frac{b_{n+k}}{2^k} \quad . \tag{16.69}$$

We now see that the logistic map has the effect of *shifting* to the left the binary digits of θ_n / π to yield θ_{n+1} / π. With each such shift, leftmost digit falls off the edge of the world, as it were, since it results in an overall contribution to θ_{n+1} which is zero modulo π. This very emphatically demonstrates the sensitive dependence on initial conditions which is the hallmark of chaotic behavior, for eventually two very close initial conditions, differing by $\Delta\theta \sim 2^{-m}$, will, after m iterations of the logistic map, come to differ by $\mathcal{O}(1)$.

16.5.3   Intermittency

Successive period doubling is one route to chaos, as we've just seen. Another route is *intermittency*. Intermittency works like this. At a particular value of our control parameter r, the map exhibits a stable periodic cycle, such as the stable 3-cycle at $r = 3.829$, as shown in the bottom panel of fig. 16.13. If we then vary the control parameter slightly in a certain direction, the periodic behavior persists for a finite number of iterations, followed by a *burst*, which is an interruption of the regular periodicity, followed again by periodic behavior, *ad infinitum*. There are three types of intermittent behavior, depending on whether the Lyapunov exponent λ goes through $\text{Re}(\lambda) = 0$ while $\text{Im}(\lambda) = 0$ (type-I intermittency), or with $\text{Im}(\lambda) = \pi$ (type-III intermittency), or, as is possible for two-dimensional maps, with $\text{Im}(\lambda) = \eta$, a general real number.
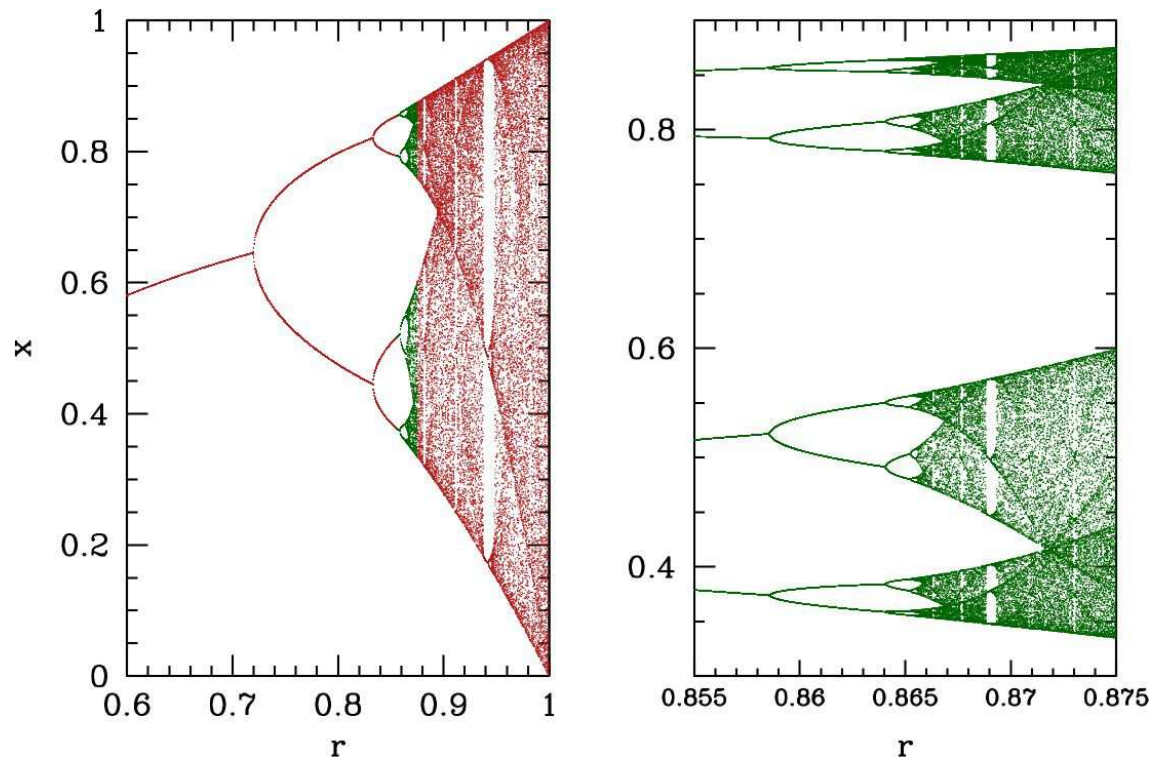
Figure 16.12: Iterates of the sine map $f(x) = r \sin(\pi x)$.

16.6 Attractors

An *attractor* of a dynamical system $\dot{\boldsymbol{\varphi}} = \boldsymbol{V}(\boldsymbol{\varphi})$ is the set of $\boldsymbol{\varphi}$ values that the system evolves to after a sufficiently long time. For $N = 1$ the only possible attractors are stable fixed points. For $N = 2$, we have stable nodes and spirals, but also stable limit cycles. For $N > 2$ the situation is qualitatively different, and a fundamentally new type of set, the *strange attractor*, emerges.

A strange attractor is basically a bounded set on which nearby orbits diverge exponentially (*i.e.* there exists at least one positive Lyapunov exponent). To envision such a set, consider a flat rectangle, like a piece of chewing gum. Now fold the rectangle over, stretch it, and squash it so that it maintains its original volume. Keep doing this. Two points which started out nearby to each other will eventually, after a sufficiently large number of folds and stretches, grow far apart. Formally, a strange attractor is a *fractal*, and may have *noninteger Hausdorff dimension*. (We won't discuss fractals and Hausdorff dimension here.)

16.7 The Lorenz Model

The canonical example of an $N = 3$ strange attractor is found in the Lorenz model. E. N. Lorenz, in a seminal paper from the early 1960's, reduced the essential physics of the coupled *partial* differential
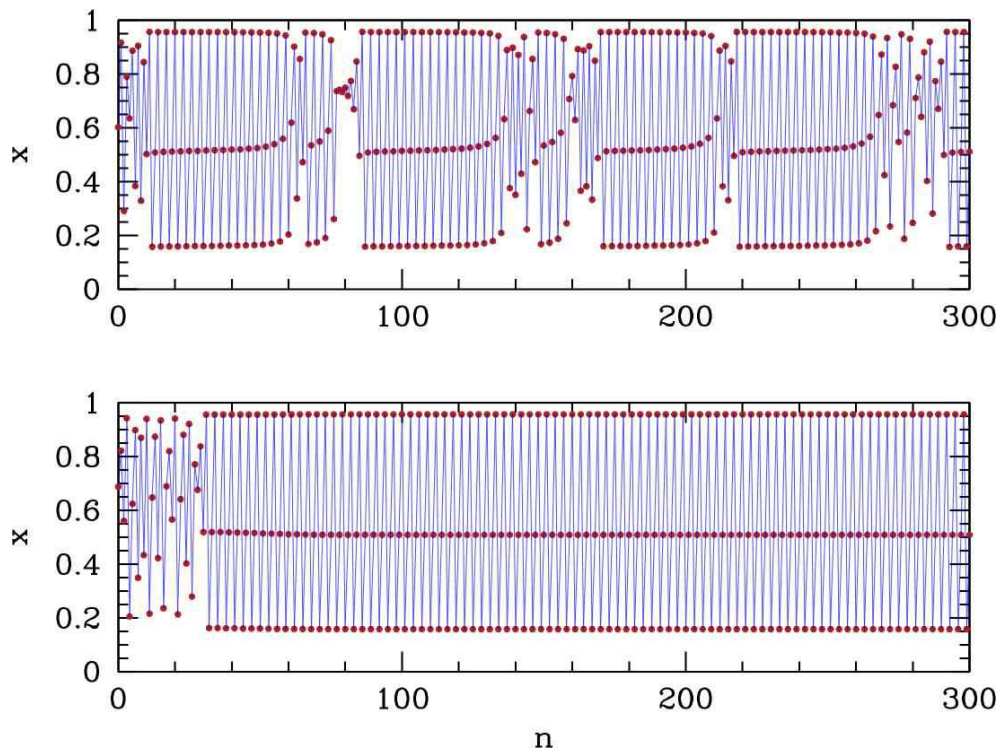
Figure 16.13:   Intermittency in the logistic map in the vicinity of the 3-cycle Top panel: $r = 3.828$, showing intermittent behavior. Bottom panel: $r = 3.829$, showing a stable 3-cycle.

equations describing Rayleigh-Benard convection (a fluid slab of finite thickness, heated from below – in Lorenz's case a model of the atmosphere warmed by the ocean) to a set of twelve coupled nonlinear *ordinary* differential equations. Lorenz's intuition was that his weather model should exhibit recognizable patterns over time. What he found instead was that in some cases, changing his initial conditions by a part in a thousand rapidly led to totally different behavior. This *sensitive dependence on initial conditions* is a hallmark of chaotic systems.

The essential physics (or mathematics?) of Lorenz's $N = 12$ system is elicited by the reduced $N = 3$ system,

$$
\begin{aligned}
\dot{X} &= -\sigma X + \sigma Y \\
\dot{Y} &= rX - Y - XZ \\
\dot{Z} &= XY - bZ \quad ,
\end{aligned}
$$
(16.70)

where σ, r, and b are all real and positive. Here t is the familiar time variable (appropriately scaled), and (X, Y, Z) represent linear combinations of physical fields, such as global wind current and poleward temperature gradient. These equations possess a symmetry under $(X, Y, Z) \rightarrow (-X, -Y, Z)$, but what is most important is the presence of nonlinearities in the second and third equations.

The Lorenz system is *dissipative* because phase space volumes contract:

$$
\mathbf{\nabla} \cdot \mathbf{V} = \frac{\partial \dot{X}}{\partial X} + \frac{\partial \dot{Y}}{\partial Y} + \frac{\partial \dot{Z}}{\partial Z} = -(\sigma + b + 1) \quad .
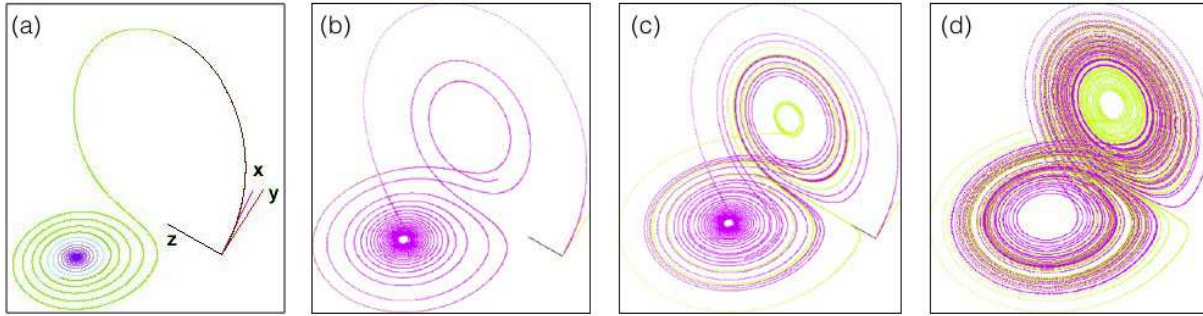$$
(16.71)

Figure 16.14: (a) Evolution of the Lorenz equations for $\sigma = 10$, $b = \frac{8}{3}$, and $r = 15$, with initial conditions $(X, Y, Z) = (0, 1, 0)$, projected onto the (X, Z) plane. The attractor is a stable spiral. (b) - (d) Chaotic regime ($r = 28$) evolution showing sensitive dependence on initial conditions. The magenta and green curves differ in their initial X coordinate by 10^{-5}. (Source: Wikipedia)

Thus, volumes contract under the flow. Another property is the following. Let

$$F(X, Y, Z) = \tfrac{1}{2}X^2 + \tfrac{1}{2}Y^2 + \tfrac{1}{2}(Z - r - \sigma)^2 \quad . \tag{16.72}$$

Then

$$\begin{aligned}
\dot{F} &= X\dot{X} + Y\dot{Y} + (Z - r - \sigma)\dot{Z} \\
&= -\sigma X^2 - Y^2 - b\left(Z - \tfrac{1}{2}r - \tfrac{1}{2}\sigma\right)^2 + \tfrac{1}{4}b(r + \sigma)^2 \quad .
\end{aligned} \tag{16.73}$$

Thus, $\dot{F} < 0$ outside an ellipsoid, which means that all solutions must remain bounded in phase space for all times.

16.7.1 Fixed point analysis

Setting $\dot{X} = \dot{Y} = \dot{Z} = 0$, we find three solutions. One solution which is always present is $X^* = Y^* = Z^* = 0$. If we linearize about this solution, we obtain

$$\frac{d}{dt}\begin{pmatrix} \delta X \\ \delta Y \\ \delta Z \end{pmatrix} = \begin{pmatrix} -\sigma & \sigma & 0 \\ r & -1 & 0 \\ 0 & 0 & -b \end{pmatrix}\begin{pmatrix} \delta X \\ \delta Y \\ \delta Z \end{pmatrix} \quad . \tag{16.74}$$

The eigenvalues of the linearized dynamics are found to be

$$\lambda_{1,2} = -\tfrac{1}{2}(1 + \sigma) \pm \tfrac{1}{2}\sqrt{(1 + \sigma)^2 + 4\sigma(r - 1)} \tag{16.75}$$

$$\lambda_3 = -b \quad ,$$

and thus if $0 < r < 1$ all three eigenvalues are negative, and the fixed point is a stable node. If, however, $r > 1$, then $\lambda_2 > 0$ and the fixed point is attractive in two directions but repulsive in a third, corresponding to a three-dimensional version of a saddle point.
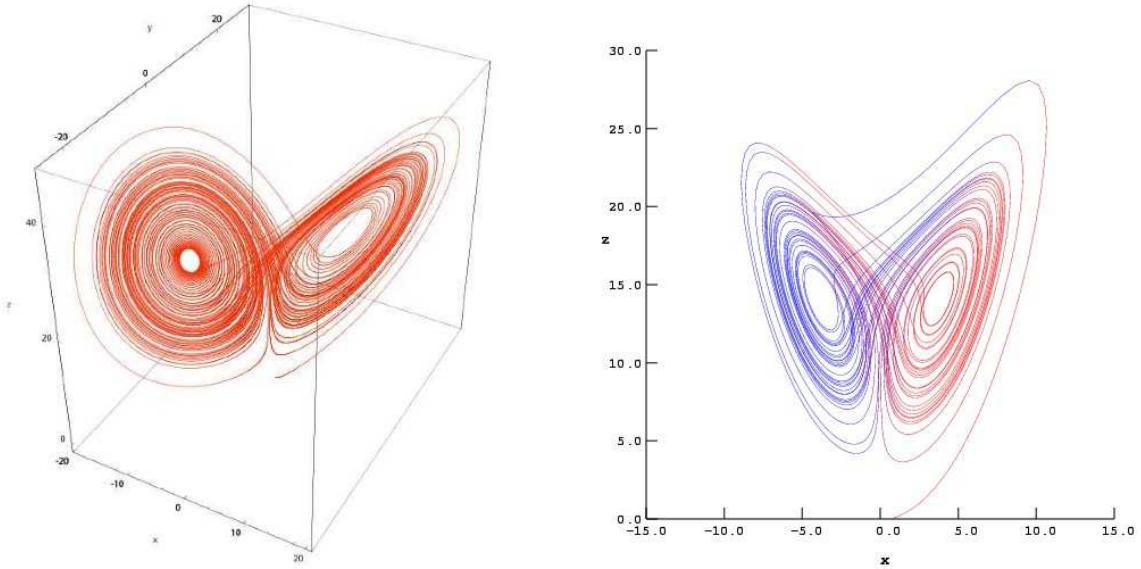
Figure 16.15:   Left: Evolution of the Lorenz equations for $\sigma = 10$, $b = \frac{8}{3}$, and $r = 28$, with initial conditions $(X_0, Y_0, Z_0) = (0, 1, 0)$, showing the 'strange attractor'. Right: The Lorenz attractor, projected onto the (X, Z) plane. (Source: Wikipedia)

For $r > 1$, a new pair of solutions emerges, with

$$X^* = Y^* = \pm\sqrt{b(r-1)} \quad , \quad Z^* = r - 1 \quad . \tag{16.76}$$

Linearizing about either one of these fixed points, we find

$$\frac{d}{dt}\begin{pmatrix} \delta X \\ \delta Y \\ \delta Z \end{pmatrix} = \begin{pmatrix} -\sigma & \sigma & 0 \\ 1 & -1 & -X^* \\ X^* & X^* & -b \end{pmatrix}\begin{pmatrix} \delta X \\ \delta Y \\ \delta Z \end{pmatrix} \quad . \tag{16.77}$$

The characteristic polynomial of the linearized map is

$$P(\lambda) = \lambda^3 + (b + \sigma + 1)\,\lambda^2 + b(\sigma + r)\,\lambda + 2b(r - 1) \quad . \tag{16.78}$$

Since b, σ, and r are all positive, $P'(\lambda) > 0$ for all $\lambda \geq 0$. Since $P(0) = 2b(r-1) > 0$, we may conclude that there is always at least one eigenvalue λ_1 which is real and negative. The remaining two eigenvalues are either both real and negative, or else they occur as a complex conjugate pair: $\lambda_{2,3} = \alpha \pm i\beta$. The fixed point is stable provided $\alpha < 0$. The stability boundary lies at $\alpha = 0$. Thus, we set

$$P(i\beta) = \left[2b(r-1) - (b + \sigma + 1)\beta^2\right] + i\left[b(\sigma + r) - \beta^2\right]\beta = 0 \quad , \tag{16.79}$$

which results in two equations. Solving these two equations for $r(\sigma, b)$, we find

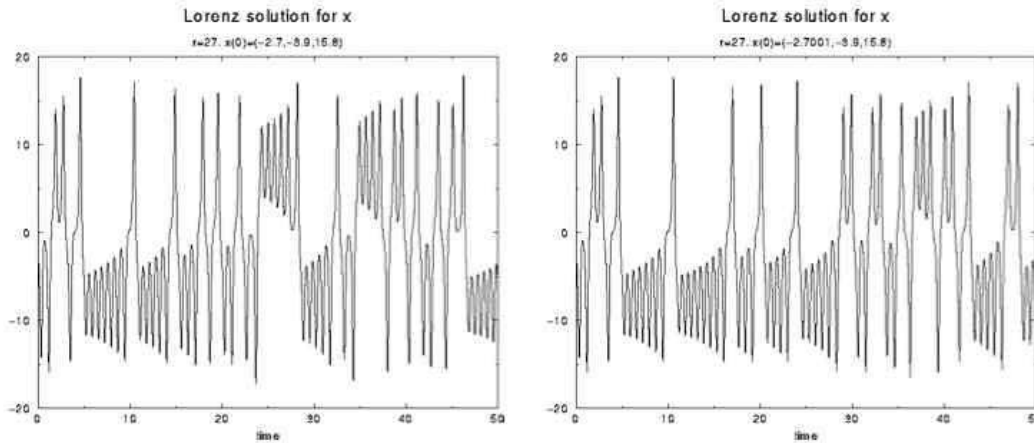$$r_{\mathrm{c}} = \frac{\sigma(\sigma + b + 3)}{\sigma - b - 1} \quad . \tag{16.80}$$

Figure 16.16: $X(t)$ for the Lorenz equations with $\sigma = 10$, $b = \frac{8}{3}$, $r = 28$, and initial conditions $(X_0, Y_0, Z_0) = (-2.7, -3.9, 15.8)$, and initial conditions $(X_0, Y_0, Z_0) = (-2.7001, -3.9, 15.8)$.

The fixed point is stable for $r \in \left[1, r_{\mathrm{c}}\right]$. These fixed points correspond to steady convection. The approach to this fixed point is shown in fig. 16.14.

The Lorenz system has commonly been studied with $\sigma = 10$ and $b = \frac{8}{3}$. This means that the volume collapse is very rapid, since $\boldsymbol{\nabla} \cdot \boldsymbol{V} = -\frac{41}{3} \approx -13.67$, leading to a volume contraction of $e^{-41/3} \simeq 1.16 \times 10^{-6}$ per unit time. For these parameters, one also has $r_{\mathrm{c}} = \frac{470}{19} \approx 24.74$. The capture by the strange attractor is shown in fig. 16.15.

In addition to the new pair of fixed points, a strange attractor appears for $r > r_{\mathrm{s}} \simeq 24.06$. In the narrow interval $r \in [24.06, 24.74]$ there are then *three* stable attractors, two of which correspond to steady convection and the third to chaos. Over this interval, there is also hysteresis. *I.e.* starting with a convective state for $r < 24.06$, the system remains in the convective state until $r = 24.74$, when the convective fixed point becomes unstable. The system is then driven to the strange attractor, corresponding to chaotic dynamics. Reversing the direction of r, the system remains chaotic until $r = 24.06$, when the strange attractor loses its own stability.

16.7.2 Poincaré section

One method used by Lorenz in analyzing his system was to plot its *Poincaré section*. This entails placing one constraint on the coordinates (X, Y, Z) to define a two-dimensional surface Σ, and then considering the intersection of this surface Σ with a given phase curve for the Lorenz system. Lorenz chose to set $\dot{Z} = 0$, which yields the surface $Z = b^{-1}XY$. Note that since $\dot{Z} = 0$, $Z(t)$ takes its maximum and minimum values on this surface; see the left panel of fig. 16.17. By plotting the values of the maxima Z_N as the integral curve successively passed through this surface, Lorenz obtained results such as those shown in the right panel of fig. 16.17, which has the form of a one-dimensional map and may be analyzed as such. Thus, chaos in the Lorenz attractor can be related to chaos in a particular one-dimensional map, known as the *return map* for the Lorenz system.
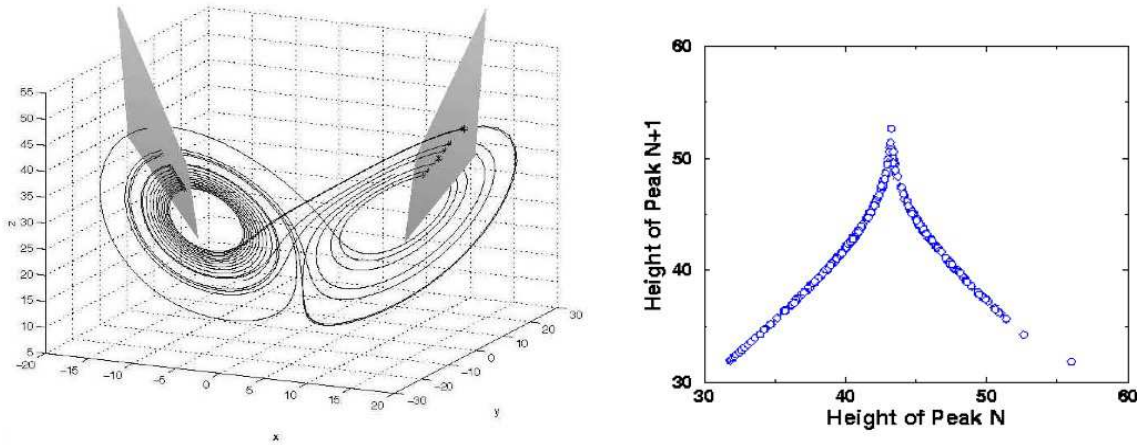
Figure 16.17: Left: Lorenz attractor for $b = \frac{8}{3}$, $\sigma = 10$, and $r = 28$. Maxima of Z are depicted by stars. Right: Relation between successive maxima Z_N along the strange attractor.

16.7.3 Rössler System

The strange attractor is one of the hallmarks of the Lorenz system. Another simple dynamical system which possesses a strange attractor is the Rössler system. This is also described by $N = 3$ coupled ordinary differential equations, *viz.*

$$
\begin{aligned}
\dot{X} &= -Y - Z \\
\dot{Y} &= Z + aY \\
\dot{Z} &= b + Z(X - c) \quad,
\end{aligned}
\tag{16.81}
$$

typically studied as a function of c for $a = b = \frac{1}{5}$. In fig. 16.19, we present results from work by Crutchfield *et al.* (1980). The transition from simple limit cycle to strange attractor proceeds via a sequence of period-doubling bifurcations, as shown in the figure. A convenient diagnostic for examining this period-doubling route to chaos is the *power spectral density*, or PSD, defined for a function $F(t)$ as

$$
\Phi_F(\omega) = \left| \int_{-\infty}^{\infty} \frac{d\omega}{2\pi} \, F(t) \, e^{-i\omega t} \right|^2 = \left| \hat{F}(\omega) \right|^2 \quad.
\tag{16.82}
$$

As one sees in fig. 16.19, as c is increased past each critical value, the PSD exhibits a series of frequency halvings (*i.e.* period doublings). All harmonics of the lowest frequency peak are present. In the chaotic region, where $c > c_\infty \approx 4.20$, the PSD also includes a noisy broadband background.
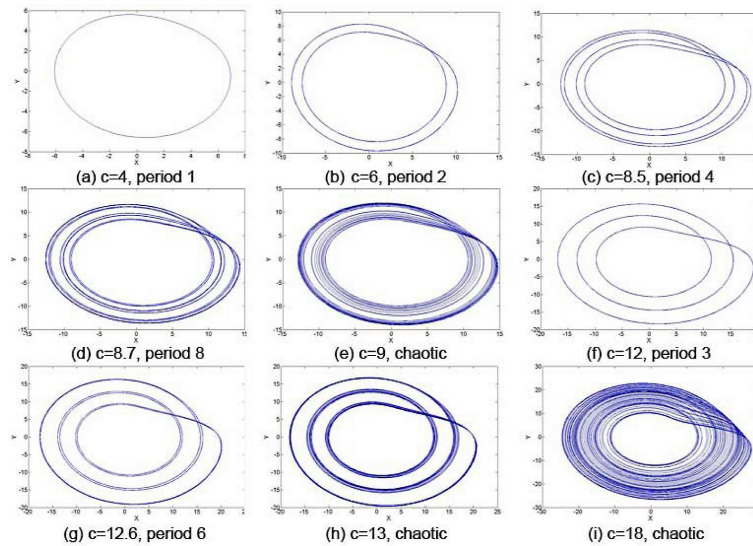
Figure 16.18: Period doubling bifurcations of the Rössler attractor, projected onto the (x, y) plane, for nine values of c, with $a = b = \frac{1}{10}$.
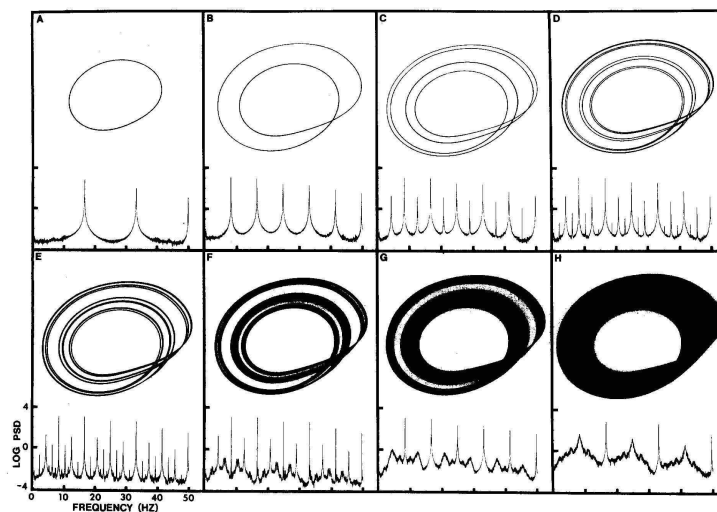

Figure 16.19: Period doubling bifurcations of the Rössler attractor with $a = b = \frac{1}{5}$, projected onto the (X,Y) plane, for eight values of c, and corresponding power spectral density for Z(t). (a) $c = 2.6$; (b) $c = 3.5$; (c) $c = 4.1$; (d) $c = 4.18$; (e) $c = 4.21$; (f) $c = 4.23$; (g) $c = 4.30$; (h) $c = 4.60$.